GIS analysis of geological surfaces orientations: the qgSurf plugin for QGIS

Mauro Alberti[1]

[1] OverIt, Strada Due, Palazzo D3 - 20090 Assago Milanofiori (MI) - Italy

Corresponding Author:
Mauro Alberti
Email address: mauro.alberti@overit.it

ABSTRACT

GIS techniques enable the quantitative analysis of geological structures. In particular, topographic traces of geological lineaments can be compared with the theoretical ones for geological planes, to determine the best fitting theoretical planes. *qgSurf,* a Python plugin for QGIS, implements this kind of processing, in addition to the determination of the best-fit plane to a set of topographic points, the calculation of the distances between topographic traces and geological planes and also basic stereonet plottings.
By applying these tools to a case study of a Cenozoic thrust lineament in the Southern Apennines (Calabria, Southern Italy), we deduce the approximate orientations of the lineament in different fault-delimited sectors and calculate the misfits between the theoretical orientations and the actual topographic traces.

Keywords: GIS, Structural geology, Field mapping, Geological surfaces

INTRODUCTION

Before the advent of remote sensing and digital elevation models, field geologists could gain a large-angle view of a particular geological zone only with the aid of geological maps. In areas with reduced outcrops, field surveys tend to produce local observations, challenging to extrapolate and integrate into more regional structures. With the availability of geographic mapping and visualization tools such as ArcGIS Pro, Google Earth, and QGIS, geologists can now virtually examine large regions. Global remote sensing mosaics with sub-meter resolutions, such as in Google and Bing web services, can allow to recognize and delineate geological structures also for large extents. Geological maps still provide ground-check truth.
This paper presents an implementation of geological tools in QGIS for inferring the structure and attitudes of geological lineaments, by taking advantage of georeferenced data, such as topographic DEMs (digital elevation models) and remote sensing images.

PLUGIN IMPLEMENTATION

qgSurf is a geological Python plugin for QGIS (QGIS Development Team, 2019), devoted to the structural analysis of field map data. Its current version is 2.1, released in the QGIS Python plugin repository in May 2019 (*https://plugins.qgis.org/plugins/qgSurf/*). It helps to extract geological information from topographic and remote sensing data, even when inaccessible to the user - provided a reliable knowledge of the local geology, the availability of ground truth data (*i.e.*, geological maps), topographic data with adequate resolution, and high-resolution remote sensing data that help to delineate, recognize and analyze geological structures of interest.

The plugin is implemented in QGIS since it is a free and open-source GIS software. Moreover, QGIS has a rich and developer-friendly environment for the creation of Python plugins: GUIs can be created with PyQt and graphics with Matplotlib. The Python API allows accessing almost all of the internal QGIS API tools. The *qgSurf* plugin takes advantage of the functionalities provided by *pygsf* *(https://github.com/mauroalberti/gsf)*, a Python library for geographical and geological computations. In turns *pygsf* relies on embedded versions of two Python modules, *mplstereonet* v. 0.5 (J. Kington, *https://github.com/joferkington/mplstereonet*) and *apsg* v. 0.6.1 (O. Lexa , *https://github.com/ondrolexa/apsg*).

There are currently four modules in qgSurf:

1. *Best fit plane*, for estimating the orientation of best-fit-plane to a sub-planar surface employing a set of topographically-defined points;
2. *DEM-plane intersection* that allows determining the theoretical intersection of a planar geological surface with the local topography;
3. *Points-plane distances*, for calculating the 3D point distances to a given geological plane;
4. *Stereonet*, with which it is possible to produce basic stereonets, thanks to embedded *mplstereonet* and *apsg* modules.

The first two tools are in a broad sense the inverse of each other. While with the *Best fit plane* tool it is possible to determine a geological attitude starting from a set of topographic points, with the *DEM-plane intersection* tool it is possible to calculate a set of topographic points starting from a geological attitude (and a single, topographic source point). For this reason, both tools require a Digital Elevation Model as a data source. In the *Best fit plane* tool, DEMs provide the elevation for the source points, while in the *DEM-plane intersection* tool they are needed for deriving the intersection points of the topography with the geological plane and optionally can also provide the elevation for the geological plane source point.

The *Points-plane distances* tool can be used to check how a set of points conforms to a geological plane, by calculating the 3D orthogonal distance from the point to the plane. Since the results are stored as a set of spatial points, they can be visualized in to investigate any spatial conformance or discrepancy with the given plane, or plot with statistical software as *R* (R Core Team, 2018) to derive the relationships between the variables. The *Stereonet* tool allows plotting geological attitudes into a stereonet. Data can be planes, lineations or fault planes with lineations.

Best fit plane

This tool calculates a best-fit-plane to a set of points, defined by the user in the map canvas or entered as numerical values. The calculations are performed via the *Singular Value Decomposition* (SVD) technique, implemented in the linear algebra submodule of *Numpy*. The result is expressed as a dip direction and dip angle. Various solutions are saved into a user-chosen

SQLite database. From that, solutions can be plotted in stereonets, deleted or exported as new or existing shapefile layers.

DEM-plane intersection

With this tool, it is possible to derive the intersections between a geological plane and a topographic surface. The geological plane is chosen by the user, by defining three parameters: the dip direction, its dip angle and a source point, whose elevation may be entered by the user or automatically extracted by the DEM. The topographic surface, represented by a DEM, is chosen by the user between those loaded in the QGIS project. It is advisable to use grids whose extent is limited to the interest area, to avoid long computation times. The computed intersections are a set of points. Generally, they present a simple, linear trend, but where the topographic surface attitude makes low angles with to the geological plane, local clusters of intersection points can also form. The user can export the result as a point shapefile.

Methodological implementation

In a GIS, topographic surfaces are generally represented as square-cell grids. Even if topographic grids do not typically present rotations, this eventuality has to be taken into consideration when treating all possible input grids. Before the 2.0 version, the Python implementations in *pygsf,* and therefore in *qgSurf,* required no grid rotations. With the 2.0 release, a new algorithm, inspired to the previous one, allows processing also grids with frame rotations.

The GDAL geotransform concept

To describe the geographical properties of a raster, GDAL, the most used open source library for GIS formats processing uses the concept of "geotransform". In essence, this is a matrix that allows deriving the geographic coordinates of a point given its pixel coordinates, and *vice versa*. An augmented matrix The geotransform is expressed with an augmented matrix:

(1)
$$\begin{bmatrix} \vec{y} \\ 1 \end{bmatrix} = \left[\begin{array}{c|c} A & \vec{b} \\ 0..0 & 1 \end{array}\right] \begin{bmatrix} \vec{x} \\ 1 \end{bmatrix}$$

so that:

(2)
$$y' = A\vec{x} + \vec{b}$$

Substituting the geotransform parameters in Eq. (1) we obtain:

(3)
$$\begin{bmatrix} x' \\ y' \\ 1 \end{bmatrix} = \begin{bmatrix} gt_1 & gt_2 & gt_0 \\ gt_4 & gt_5 & gt_3 \\ 0 & 0 & 1 \end{bmatrix} \begin{bmatrix} x \\ y \\ 1 \end{bmatrix}$$

The linear equations for the transformed coordinates are:

(4)
$$\begin{aligned} x' &= gt_1 x + gt_2 y + gt_0 \\ y' &= gt_4 x + gt_5 y + gt_3 \\ 1 &= 0 + 0 + 1 \end{aligned}$$

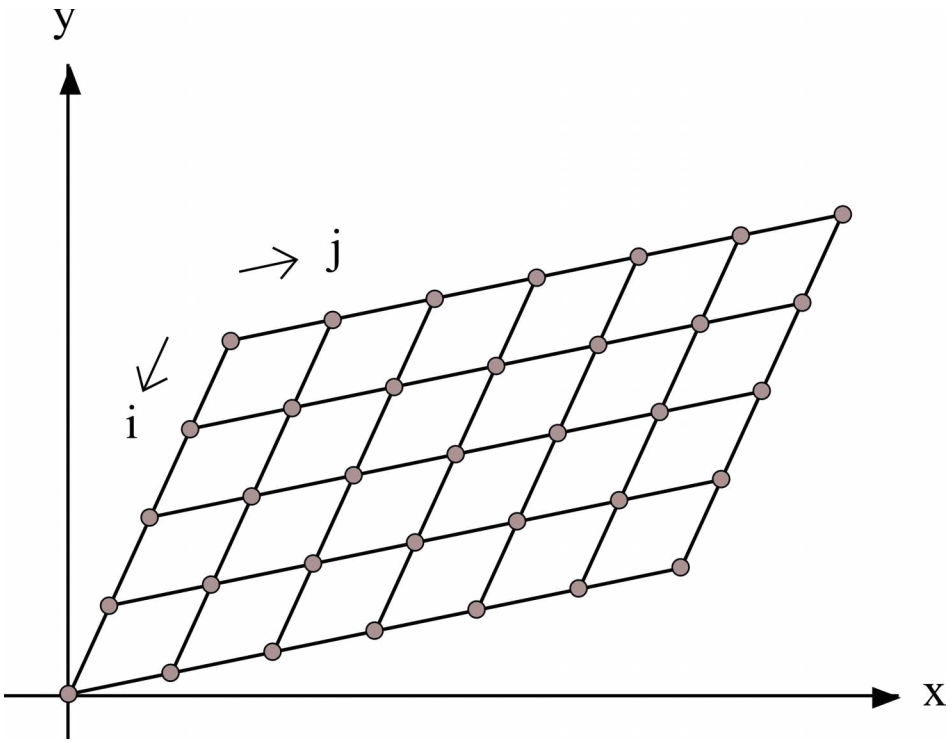

Figure 1: Example of an orthogonal grid transformed by an affine transformation.

From the equation set in (4), we can observe that gt_0 and gt_3 parameters represent grid offsets in the x - and y- directions respectively, gt_1 and gt_5 are scaling factors for x- and y- directions, while gt_2 and gt_4 represent rotations/skewing. In the general case, an orthogonal grid can be transformed by a geotransform into a grid whose x and y-axes are no longer orthogonal (Fig. 1).

Point intersections determination methodology

To determine the plane-DEM intersections the geometrical problem is simplified from 3D to 2D. We consider the geometric traces of the plane and the topographic surface with two sets of parallel vertical planes, the former oriented parallel to the final *j*- grid axes orientations, the latter set parallel to the last *i*- grid axis orientation (Fig. 1). Each plane of the set contains a grid point row (for the *j*-parallel planes) or column (for the *i*-parallel planes). The points correspond to the final grid cell centers.
We consider now a single vertical plane with a *j*-parallel orientation (Fig. 2, corresponding to a vertical section). We have evenly spaced final cell centers along the plane, where the spacing does not necessarily correspond to the original geotransform cell sizes, given that, as a general case, the grid can also be distorted in the axis lengths. This spacing is however constant within each set of vertical planes. We can compute it as the distance between the first and second transformed cell centers. When there is no grid skewing, only a rigid-body rotation or no rotation at all, the spacing will be equal to the original grid cell sizes.

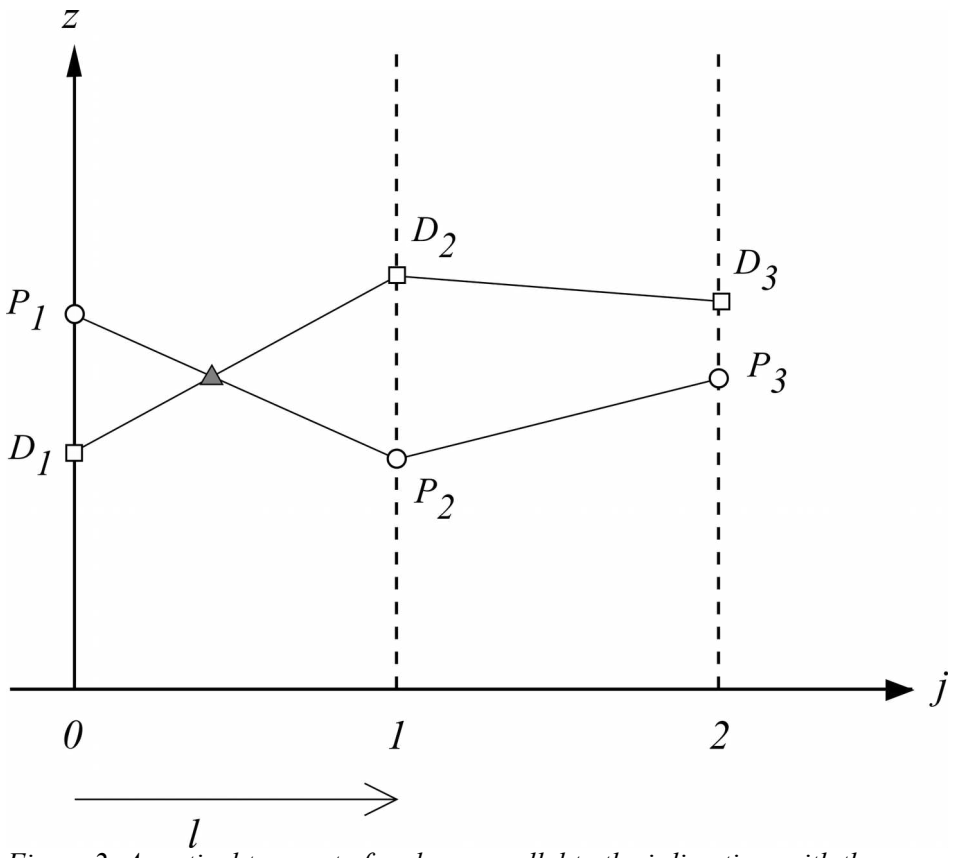

Figure 2: A vertical transect of a plane parallel to the j-direction, with the examples of intersecting plane (P points) and DEM (D points) traces.

Within a single vertical plane, we consider its intersections with the DEM and the plane surfaces, at each transformed cell centers. The point intersection with the DEM corresponds to the DEM height for that cell, while the plane intersections are calculated given the plane equation and the considered cell center point coordinates. Knowing the DEM and plane height for each cell center along a vertical plane, we can determine the plane-DEM intersection between two consecutive cell centers, as described below.

We have a valid plane-DEM intersection point between two consecutive cell centers (for instance j=0 and j=1 in Fig. 2) when the relative z positions of the plane and the DEM traces switch between the two considered cell centers. On the other hand, when the plane line is always higher (or lower) than a DEM line, there is no intersection (*e.g.*, j=1 and j=2 in Fig. 2).

When at a cell center line and DEM points coincide, it corresponds to an intersection point. The height equations for the DEM and the plane are:

(5)
$$x' = gt_1 x + gt_2 y + gt_0$$
$$y' = gt_4 x + gt_5 y + gt_3$$
$$1 = 0 + 0 + 1$$

where q_p is the plane elevation at point (x, y), q_d is the grid z value, m_d is the angular coefficient of the DEM trace (for the given direction), and m_p is the angular coefficient of the plane trace in the considered direction.

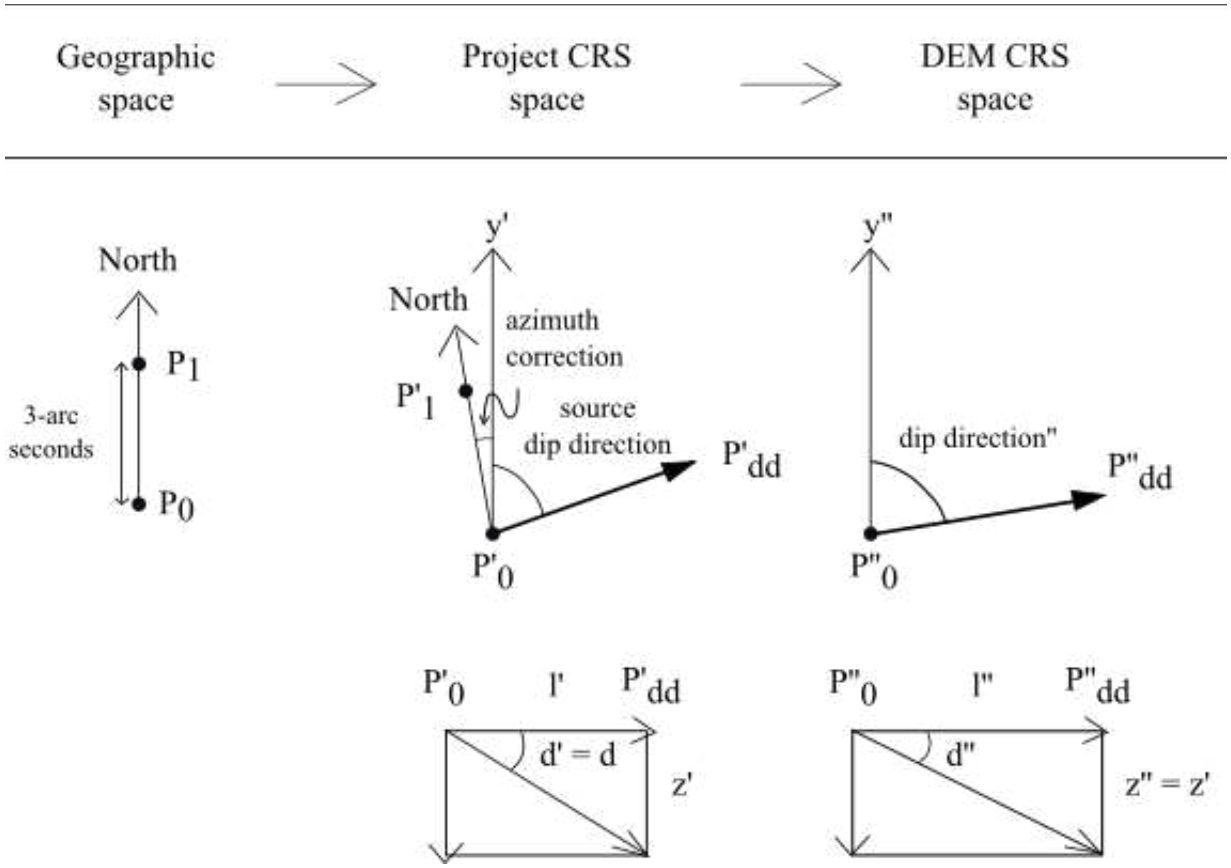

Figure 3: Transformation steps from geographic to DEM CRS space for the DEM-plane intersection tool.

At an intersection point we have:

(6)
$$m_d x' + q_d = m_p x' + q_p \Rightarrow$$
$$(m_d - m_p)x' = q_p - q_d \Rightarrow$$
$$x' = \frac{q_p - q_d}{m_d - m_p}$$

where x' is the distance of the intersection point from the left cell center. The array coordinate of the intersection point is therefore equal to:

(7)
$$\frac{x'}{cellsize'} = i'[0 \rightarrow 1]$$

where *cellsize'* is equal to the geotransformed cell spacing in the considered direction and i' is the array coordinate in the considered direction, that is transformed into geographic coordinates by applying the geotransform, thus solving the investigated problem.

Practical determination of DEM-plane intersections

The projection used for a particular GIS project may differ from the CRS of the DEM chosen for the determination of the intersection. This fact has two practical implications:

1. in the projection used by the current project, the top direction (*y*-axis direction) can be not parallel to the geographic North;
2. in the case of project-DEM projections difference, there can be a variation of the orientations and length of corresponding lines between the two projective systems.

We need therefore two preliminary corrections applied to the geological plane attitude, the former related to the geographic North disorientation angle (with regards to the project *y*-axis), the latter required by the change from project to DEM CRS, with the related impact on both the length and the orientation of a segment parallel to the geological plane dip-direction (cf. Fig. 3). These two corrections are described in *Appendices 1* and *2* respectively.

Points-plane distances

This tool calculates the orthogonal, 3D distances between a set of 3D points and a geological plane, expressed in the same way as in the *DEM-plane intersection* tool. The collection of 3D points is stored in a GIS layer, with three fields storing respectively the *x*, *y* and *z* components. The result is represented by a GIS point layer, in shapefile format, with a field added with the distance results. This tool can be used to assess the spatial variation in the fit of points to a geological plane, by GIS visualization or statistical analysis in Cartesian plots.

Stereonet

It allows plotting geological planes or lineations into a stereonet, with user-defined graphics style. Stereonets can be exported as graphical files. To create stereonets, it makes use of an embedded version of the *apsg* library by Ondrej Lexa.

AN EXAMPLE OF GEOLOGICAL ANALYSIS WITH QGSURF

Introduction

We analyze a Cenozoic thrust lineament, located in the Southern Apennines (Italy), more precisely in Northern Calabria, to the East of San Lorenzo Bellizzi town (Fig. 4).
The thrust has a general NNW-SSE orientation, and it is segmented into a few disconnected segment to the North of San Lorenzo Bellizzi (Fig. 4, *T1-3* segments), while in the southern sector it is more continuous, with some minor offsets due to later faulting (Fig. 4, *T4* segment). The footwall of the thrust is constituted by Jurassic-Cretaceous carbonatic platform limestones, of the Pollino Unit, that outcrops also in the Mt. Pollino mountain range, to the West of the investigated area (Ghisetti & Vezzani, 1982). In the hangingwall, there are marine Mesozoic sediments and meta-sediments, of the *Crete Nere* and *Frido* Formation of the Liguride unit (Vezzani *et al*., 2010, cf. Fig. 30 therein), named "*Unità del Flysch Calabro-Lucano*" in Monaco *et al*. (1994). High-angle faults offset the thrust, probably normal faults related to the recent (? < 0.7 Ma) distensive regime active in this region, with sub-horizontal sigma-3 axis oriented NE-SW (e.g., Frepoli & Amato, 2000).

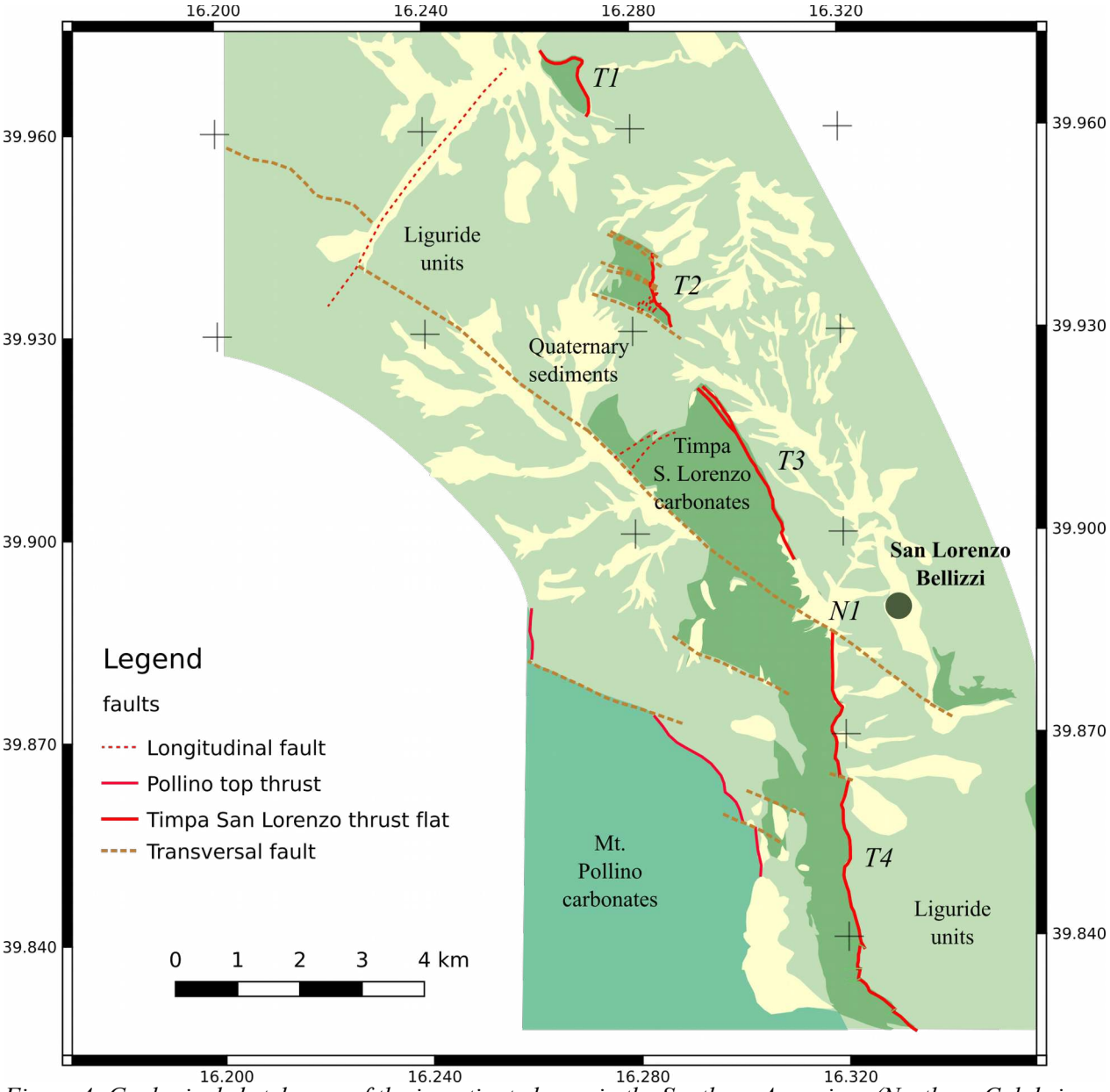

Figure 4: Geological sketch map of the investigated area in the Southern Apennines (Northern Calabria, Italy). Simplified from Monaco et al. (1994) and 1:100,000 "221- Castrovillari" Italian Geological Survey geological sheet. Map created with QGIS.

The carbonatic rocks in the thrust footwall constitute stiff and erosion-resistant volumes, mainly affected by faulting. Their low erodability in the semi-arid Southern Italy climate, pale gray exterior alteration color and thick stratification allows to distinguish them from the neighboring rock units in remote sensing images (cf. Figs. 5 and 6 from Google Maps service). 3D visualizations, with ArcGIS Pro or Google Maps, of the outcropping traces of this thrust lineament, suggest sub-planar geometries for its segments, with reduced orientation changes due to later normal faults, as recognizable for the normal fault located to the West of *San Lorenzo Bellizzi* town (*N1* in Fig. 4, see also Figs. 5 and 6).

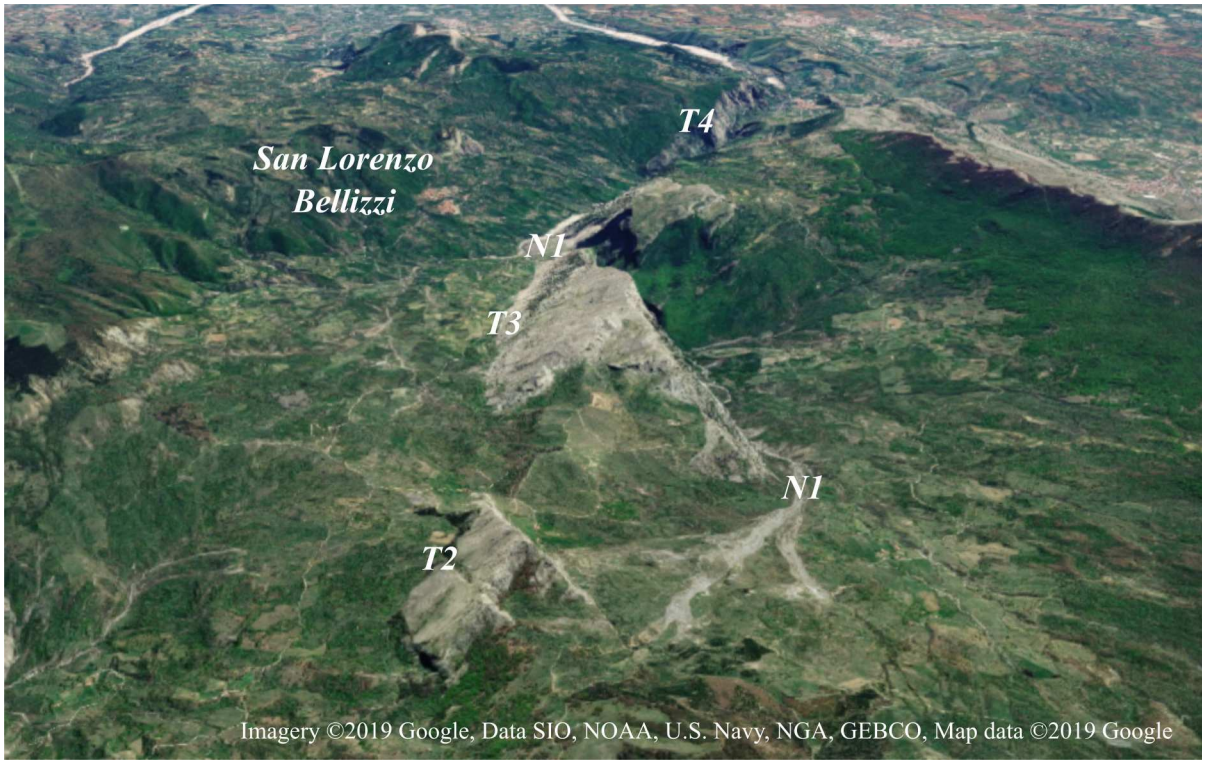

Figure 5: Investigated area viewed from North (segments T2, T3, T4 and N1 as in Fig. 4). The investigated tectonic contact is NNW-SSE oriented and dips at low-angle to the East. A set of NW-SE lineaments dissecting the primary contact as well as the basal carbonatic volumes, with downward movements to the West, is also evident. Google Maps background. Map data © 2019 Google.

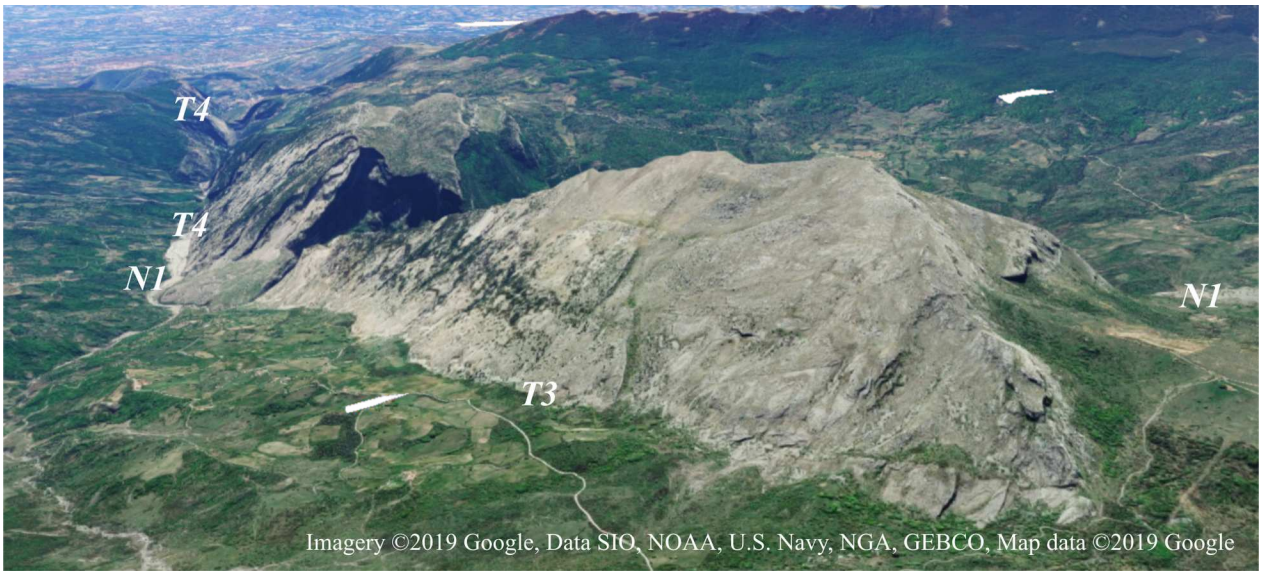

Figure 6: Close-up of the Timpa di San Lorenzo zone (segment T3 and the northern part of T4 as in Fig. 4), as viewed from North-East. Both the northern and the southern structures correspond to monoclinal surfaces in the carbonatic rocks (grey color) that we interpret as close remnants of the original tectonic contact. Map data © 2019 Google.

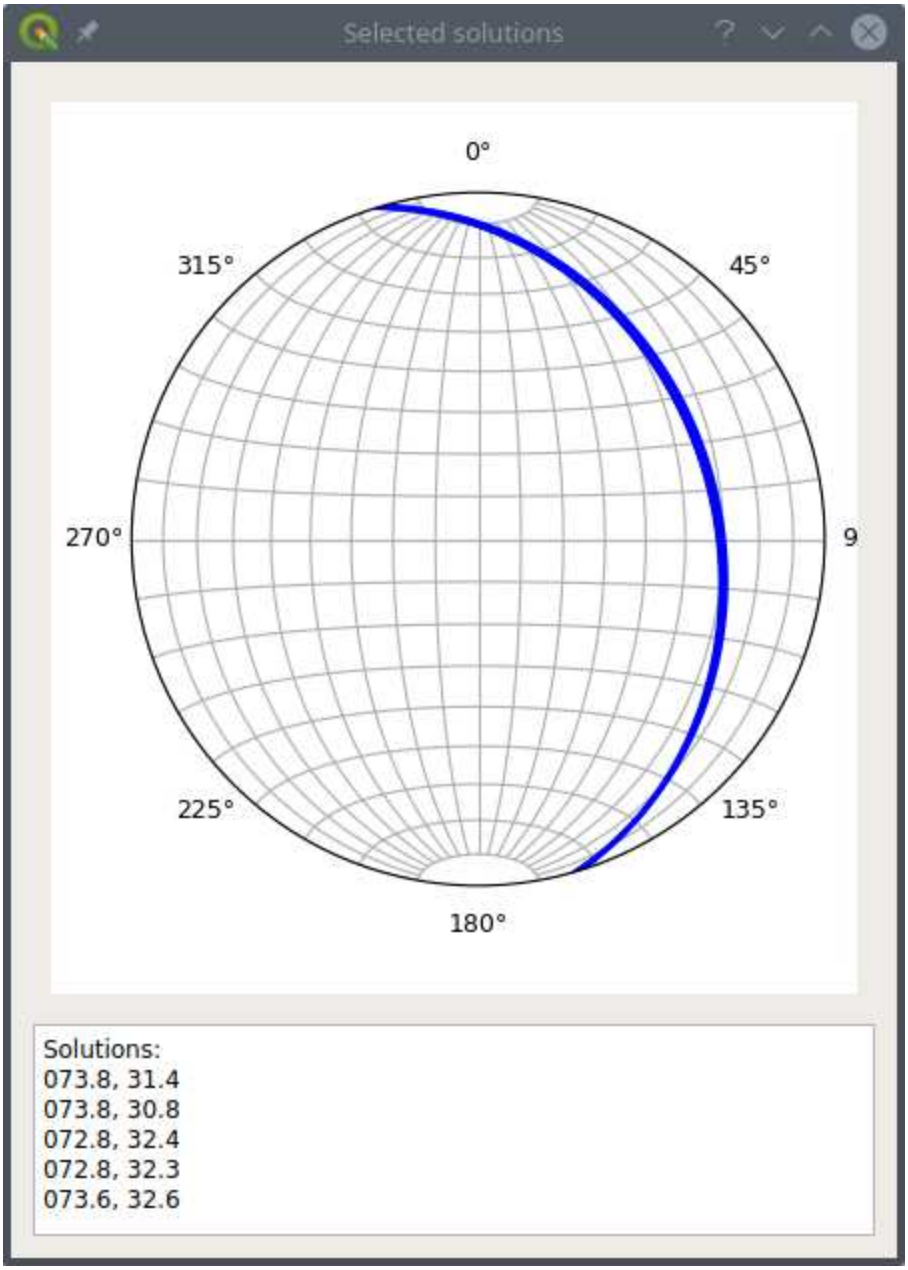

Figure 7: Best fit plane solutions obtained for the northern Timpa di San Lorenzo monoclinal surface, using five sampling cases. The obtained mean value is 073°/32° (dip direction/dip angle).

The analyses were performed by integrating local geological information as mapped in Monaco *et al*. (1994) and the Italian Geological Survey 1:100,000 sheet "221 - Castrovillari", while topographic data derived from 10 m resolution *tinitaly* DEM, released by ING (Tarquini & Nannipieri, 2017). Four tiles from this DEM were merged using Saga GIS (Conrad *et al*., 2015), with the mosaicking function and bilinear interpolation resampling. In order to reduce calculation times for the operations of the plane-DEM intersection, the merged grid was resized to the interest region extent. Remote sensing background is provided by Bing and Google services, loaded in QGIS via the *QuickMapServices* plugin.

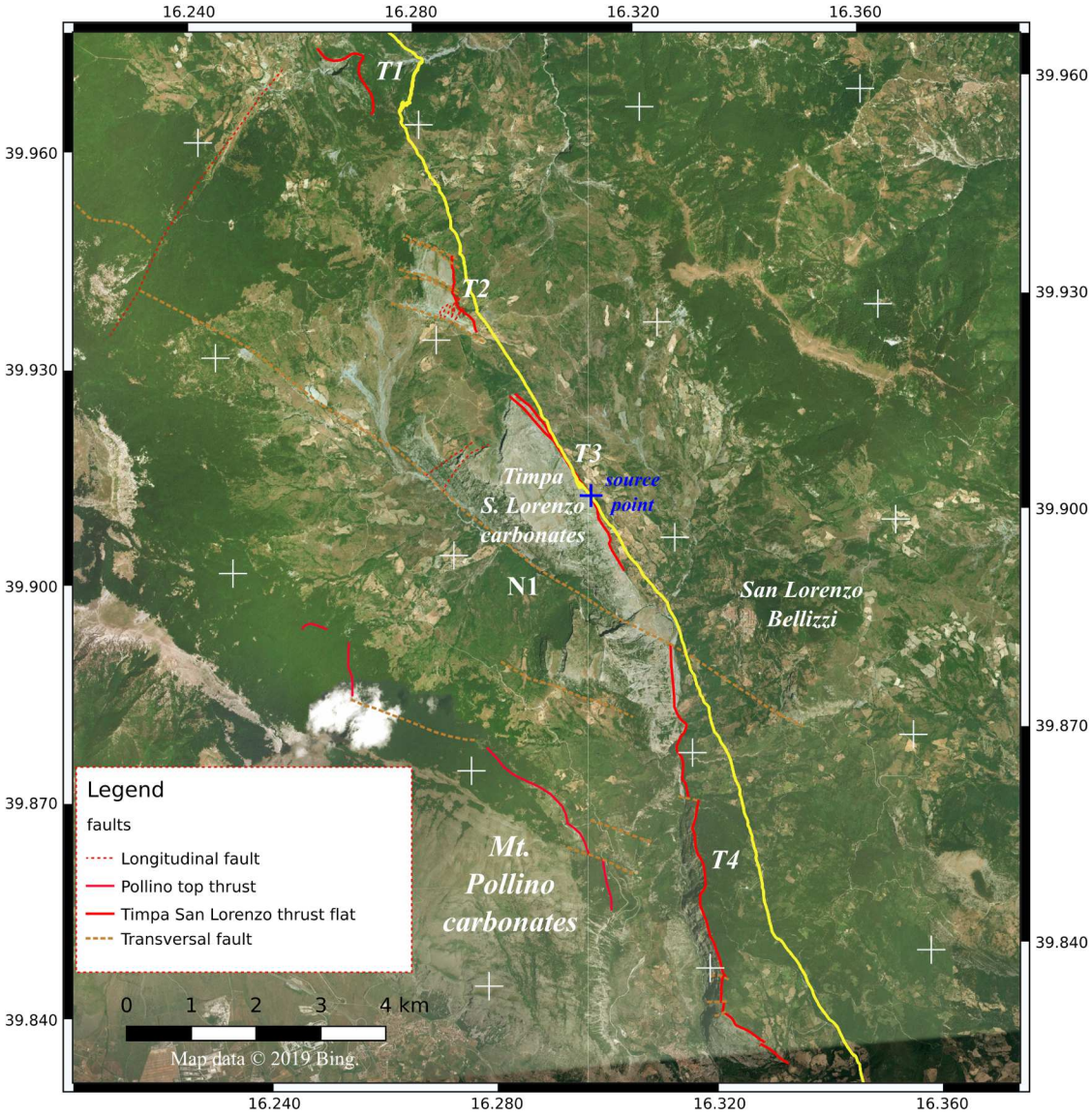

Figure 8: Map representing both the thrust segments and the DEM-plane intersections-derived (yellow) obtained for the northern sector of the thrust, using a solution of 072°/39° (blue cross is the source point for the DEM-plane intersection calculation). Remote sensing background is Bing web service. Map data © 2019 Bing.

The carbonatic rocks outcrops and the major fault lineaments were digitized in QGIS using the Bing and Google Maps services as background, and the georeferenced versions of Monaco *et al.* (1994) geological map and the "221 - Castrovillari" geological sheet as ground-truth sources.

Geological analyses

The thrust trace is made up by a few segments, in the northernmost sector disconnected and with short lengths (*T1* and *T2* segments in Fig. 4 and followings), more continuous in the central and southern parts (*T3* and *T4* segments in Fig. 4 and followings).

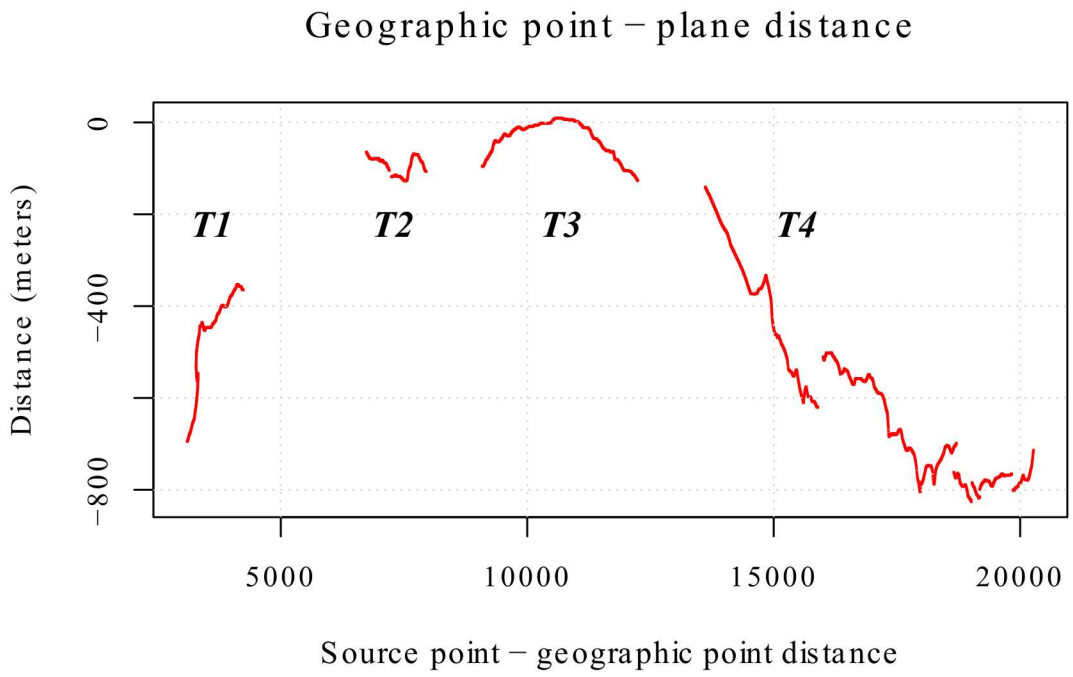

Figure 9: 3D distances between the topographic points of the thrust surfaces and the 072°/39° oriented geological plane versus the topographic point distance from the source point (see Fig. 8). Thrust segments (T1-4) names are as in Fig. 4. Negative distances indicate points under the geological plane.

Between the northernmost carbonatic outcrops, sediments of the *Flysch Calabro-Lucano* or alluvium are mapped in the considered geological maps. The visual investigation of the upper surface of these bodies in a 3D scene of ArcGIS Pro suggests sub-planar geometries with limited orientation changes for the segments from *T2* to *T4* (Figs. 5 and 6). The *Timpa di San Lorenzo* segment (*T3*) and the segment south of *San Lorenzo Bellizzi* (*T4*) both present monoclinal, East-dipping surfaces that are possibly remnants of the original thrust surface. The northern monoclinal appears to be less weathered and eroded than the southern surface. The two monoclinal surfaces show a slight difference between their orientations, due to an NW-SE fault (*N1*), dissecting the thrust surface (Figs. 4 and 6).
By using the *Best fit plane* tool on the northern, less weathered monoclinal surface (*T3*, cf. Fig. 6, steep surface in the foreground), a mean attitude of 073°/32° is obtained (Fig. 7). Due to its more intense weathering, we do not calculate the correspondent for the southern monoclinal surface (northern sector of *T4*). After having determined the possible orientation of the northern sector thrust surface, we now turn to the examination of the topographic traces of the thrust, by determining, with the help of the *DEM-plane intersection* tool, the approximated orientations of

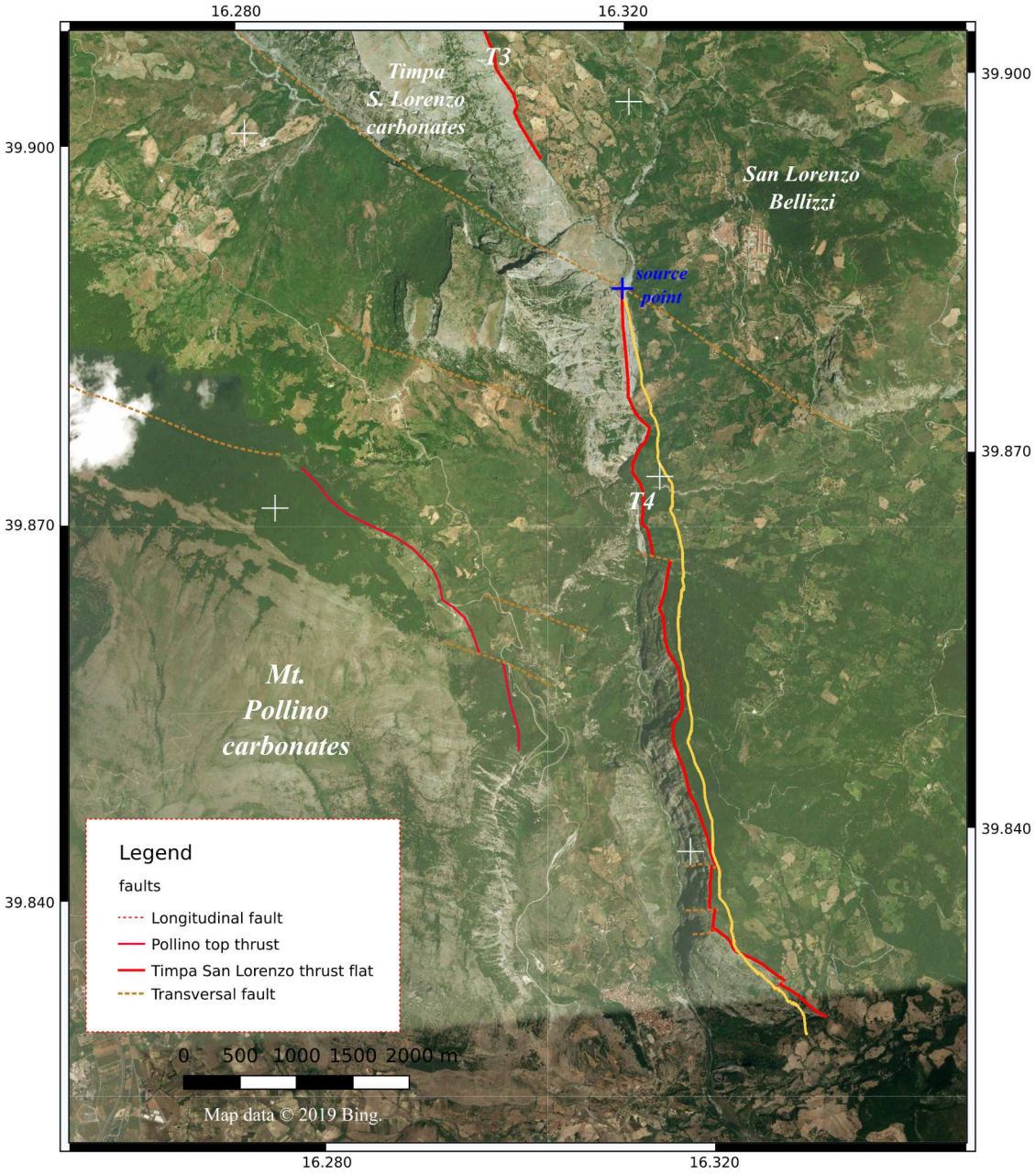

Figure 10: DEM-plane intersections (yellow) obtained for the southern sector of the thrust (T4), using a solution of 082°/40°. Remote sensing background is Bing web service. Map data © 2019 Bing.

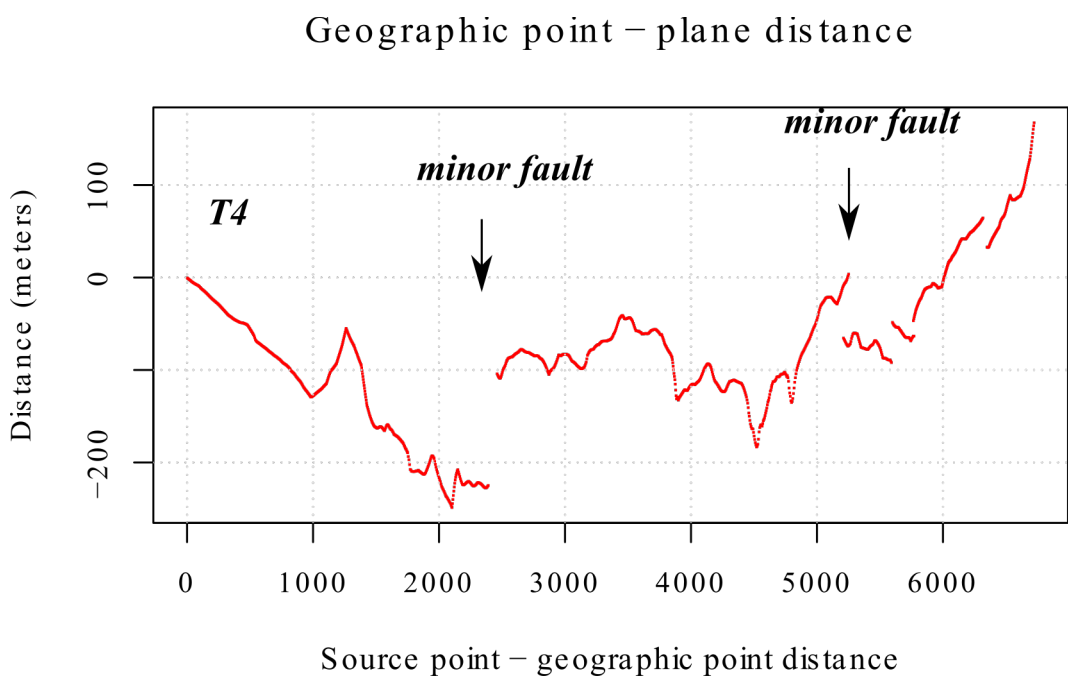

Figure 11: 3D distances between the topographic points of the southern segment of the thrust (T4) and the 082°/40° oriented geological plane versus the topographic point distance from the source point (see Fig. 10). Negative distances indicate points under the geological plane, positive points above the geological plane.

the thrust. As previously described, this tool allows determining the intersections of a geological plane with a topographic surface. By trial-and-error, it is possible to estimate the orientations of a set of sub-planar lineament segments. We first examine the northern sector trace, in correspondence of the possibly fresh thrust exposure previously examined, that presented an average orientation of 073°/32° by using the *Best fit plane* tool. The best approximation of the geological traces, at least for the northern sector of the thrust trace, is produced by a 072°-39° oriented plane (dip direction-dip angle), using a *source point* located near the center of the *T3* fault segment (Fig. 8). This ENE-dipping orientation is very similar to the one obtained for the monoclinal surface with the *Best fit plane* tool, except a slightly larger dip angle (7° higher). The misfit of the theoretical trace with the actual one increases as we move farther from the chosen *source point* (Fig. 8). Moreover, the actual trace is always located SW of the theoretical one, indicating that the fault surface is located below the theoretical 072°-39° plane, and that could have a slightly curved geometry, or that it is shifted below the theoretical plane by minor faults. The fit for the *T1* segment is generally reduced, while for the *T4* segment it is less and less satisfactory as we move southward (Fig. 8).

We may quantify the fit between the chosen geological plane and the actual tectonic contact through the *Point-plane distances* tool. As a geographic source data, we need a point layer representing the locations of the investigated lineament. The line segments of the thrust were therefore converted to points in a new point layer, their geographic coordinates and DEM-derived elevation values added in new fields with the help of Saga GIS.

Figure 9 expresses the quantitative relationships between the 3D perpendicular distances of the trace points from the geological plane *versus* the distances of the trace points from the *source point*. While the *Timpa di San Lorenzo* segment traces (*T3*) and the traces of the segment to the

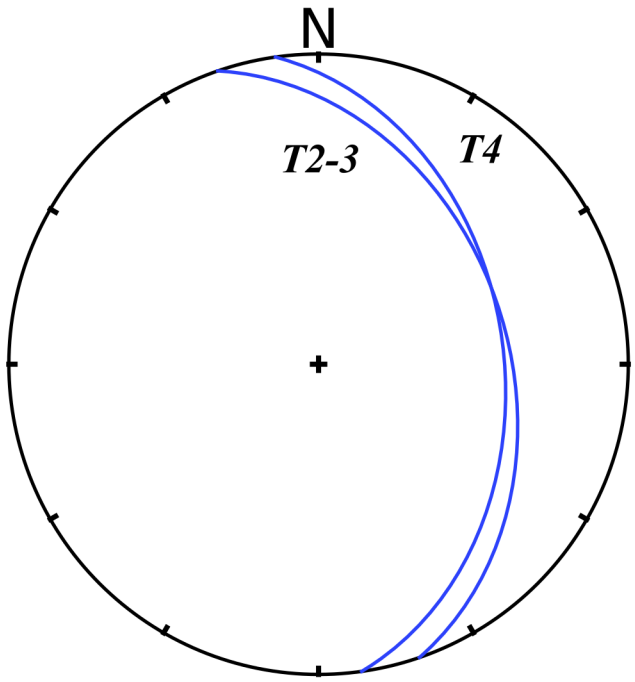

Figure 12: Stereonet representing the two first-order orientations of the northern (T2-3: 072°/39°) and southern (T4: 082°/40°) sectors of the thrust surface.

North (*T2*) are located less than 100-150 m from the geological plane, the northernmost sector (*T1*) as well as the southern sector (*T4*) present distances in excess of 150-200 m, up to 824 m (the negative sign indicate that the topographic points are *below* the geological plane) (Fig. 9). We note that the fit of the traces from the geological plane decreases in a curvilinear or linear way from the central point of the *T3* segment (*Timpa di San Lorenzo* sector). The northernmost sector (*T3*) has a large misfit with the 072°/39° plane, with values rapidly increasing as going northward. The southernmost sector (*T4*) has increasing misfit values going southwards, presenting both linear trends and offsets due to local faults. Towards its southern extreme, the misfit stabilizes at around 800 m below the theoretical plane. The linear trends in the misfit, increasing or decreasing, are probably related to sectors with a sub-planar geometry that is oriented at an angle to the geological plane. The actual trend inclination would depend on a few variables, such as the local plane disorientation and the varying topographic heights of the traces. When trying to model the southern part (*T4* as in Fig. 4), the same *DEM-plane intersection* procedure used in the northern sector case, suggests a good approximation for the geological trace for a plane with an orientation 082°- 40° (dip direction-dip angle) (Fig. 10). Plotting the distances of the trace points from the source point versus the 3D perpendicular distance of the trace point from the geological plane, we note a better fit between the theoretical plane and the actual fault trace, within +/- 200 m from the geological plane (Fig. 11). The fault surface is segmented in at least three major segments, with slightly different orientations as reflected by the difference trends visible in Fig. 11, resulting from fault tilting or possibly by inter-segment folding.

We can, therefore, as a first approximation, model the examined *Liguride-Pollino* units tectonic contact segments as made up by two principal subplanar surfaces, offset by later transversal faults. The two sub-planar surfaces have the same dip angle (around 40°) but differ in orientation by around 10° (see plot obtained with the *Stereonet* module in Fig. 12).

CONCLUSIONS

The use of 3D visualization of combined topographic and remote sensing data in GIS softwares allows to revise and extrapolate field-based geological interpretations. GIS-based quantitative tools allow deriving estimates of geological surfaces attitudes also in a remote way. The quantitative analysis of the distances between geological traces and estimated geological planes is sensitive also to limited orientations variations, due for instances to later faulting, thus potentially enabling detailed analyses of the orientation variations of geological surfaces.

ACKNOWLEDGMENTS

Statistical analyses were performed with R.
Latex formulas were created with DAUM Equation Editor:
http://s1.daumcdn.net/editor/fp/service_nc/pencil/Pencil_chromestore.html

APPENDICES

Appendix 1

Correction for the disorientation of geographic North in current project CRS

When we consider the orientation of geological planes, we are referring to it as the azimuth of the plane dip direction to the geographic North. Since the algorithmic calculation refers to the Cartesian *y*-direction (up-direction) in the current (*i.e.*, project-defined) projection, we have to correct the user-provided orientation for the horizontal angular disorientation between the geographic North and the *y*-axis. Moreover, in the general case, this angular disorientation cannot be assumed constant for all of the investigated area (*i.e.*, the DEM extent).
In order to simplify the correction calculation, the considered location is the user-defined *source point* of the geological plane. From a practical point of view, this is also a location of significant interest for the user, so that it is optimal to obtain the maximum intersection correctness in its neighborhood. In practical cases, the obtained correction is generally minimal (less than 1°), so its variation in the full DEM extent can also be considered irrelevant (also considering all involved analytical errors). The angular disorientation calculation is as follows:

1. the user-defined source point is converted from the original project CRS to a latitude-longitude framework;
2. in the latitude-longitude framework, a second dummy point is created just North of the source point, at a distance of around 90 meters (3 arc-seconds);
3. the source and the dummy North points are projected in the project CRS;
4. in the project CRS, the angle between the projected North-oriented segment and the y-axis is calculated;
5. the azimuth correction (angle between geographic North and y-axis, measured clockwise) is added to the user-provided geological plane dip-direction.

Appendix 2

Correction for the line transformation between project CRS and DEM CRS

Since, for algorithmic simplicity, the calculations to derive the intersection points are implemented in the DEM CRS space, we have to consider the impact of CRS change, i.e., to DEM CRS from project CRS, on the geological plane attitude.
A segment can be transformed in two way: its spatial orientation may change, as well as its length. When the reference segment (parallel to the dip direction of the geological plane) changes orientation, it requires a correction of the azimuth of the dip direction, similarly to the previously described azimuth correction for the geographic North disorientation in the project CRS. When there is a change in the horizontal length of the reference segment, it impacts the dip angle in the DEM CRS, since the depth is not distorted proportionally by the re-projection. The correction is derived in a way similar to the previously described corrections (cf. Fig. 3). A segment, parallel to the (North-corrected) geological plane dip-direction and with a starting length of 100 distance units (e.g., meters) is created in the project CRS space using the methods for vector manipulation made available in the pygsf library. It is projected in the DEM CRS space, and its new orientation and lengths are extracted. This two information is used to update the geological plane dip direction and angle.

REFERENCES

Conrad, O., Bechtel, B., Bock, M., Dietrich, H., Fischer, E., Gerlitz, L., Wehberg, J., Wichmann, V., and Böhner, J. (2015): System for Automated Geoscientific Analyses (SAGA) v. 2.1.4, Geosci. Model Dev., 8, 1991-2007, doi:10.5194/gmd-8-1991-2015.

Frepoli, A., Amato, A., 2000. Spatial variation in stresses in peninsular Italy and Sicily from background seismicity. Tectonophysics, 317, 109-124.

Ghisetti F., Vezzani, L., 1982. Strutture tensionali e compressive indotte da meccanismi profondi lungo la Linea del Pollino (Appennino meridionale). Boll. Soc. Geol. It., 101, 385-440.

Monaco C., Tortorici L., Morten L., Tansi C., Critelli S., 1994. Geologia del versante nord-orientale del Massiccio del Pollino (Appennino Meridionale): carta geologica alla scala 1:50.000.In Geologia delle Aree di Avanpaese (Riassunti) - Società Geologica Italiana - 77a Riunione Estiva, Congresso Nazionale. Proceeding of Società Geologica Italiana - 77a Riunione Estiva, Congresso Nazionale, 257-257.

QGIS Development Team, 2019. QGIS Geographic Information System. Open Source Geospatial Foundation Project. http://qgis.osgeo.org.

R Core Team (2018). R: A language and environment for statistical computing. R Foundation for Statistical Computing, Vienna, Austria. URL https://www.R-project.org/.

Tarquini S., Nannipieri L., 2017. The 10m-resolution TINITALY DEM as a trans-disciplinary basis for the analysis of the Italian territory: Current trends and new perspectives. Geomorphology 281, 108-115.

Vezzani, L., Festa A., Ghisetti F. C., 2010. Geology and Tectonic Evolution of the Central-Southern Apennines, Italy. The Geological Society of America Special Paper 469. ISBN: 978-0-8137-2469-0.